Analytical model for predicting coverage in suspension waterjet shot peening and its influence on fatigue

Materials Research Express

PAPER

Analytical model for predicting coverage in suspension waterjet shot peening and its influence on fatigue

Yongtao Ma[1], **Chunfan Li**[1], **Ning Sun**[1,*], **Lanrong Liu**[1,*], **Chunsheng Lu**[2], **Junlong Wang**[1] and **Bin Zhang**[1]

[1] School of Mechanical and Power Engineering, Zhengzhou University, Zhengzhou 450001, People's Republic of China
[2] School of Civil and Mechanical Engineering, Curtin University, Perth 6845, Australia
* Authors to whom any correspondence should be addressed.

E-mail: 202022202013969@gs.zzu.edu.cn and llrong@zzu.edu.cn

Keywords: abrasive waterjet peening, analysis model, coverage, residual stress, roughness

OPEN ACCESS

RECEIVED
14 March 2023

REVISED
3 June 2023

ACCEPTED FOR PUBLICATION
19 June 2023

PUBLISHED
14 July 2023

Abstract

Suspension waterjet peening is an emerging technology for surface modification. Coverage is a key factor affecting the integrity of a modified material surface, however such an experimental method that can be utilized for precise control has not yet been established. To determine the numerical value of coverage after surface peening treatment, In this paper, a coverage analytical method was proposed and then verified by the results through experiments. Furthermore, to explore the impact of high coverage on surface integrity, a large-scale coverage peening modification was performed on 18CrNiMo7-6 carburized steel specimens using a specialized suspension waterjet equipment. The results indicate that coverage has a significant impact on roughness and compressive residual stress field, with the highest improvement on surface and their maximum values reaching 51.6% and 24.7%, respectively. It is shown that the fatigue performance of the specimens can be significantly enhanced.

1. Introduction

Water jet shot peening is a new technology for surface modification [1]. It uses the high-speed kinetic energy of water jets to drive solid shots that strike the target material, creating plastic deformation and a compressive residual stress (CRS) field on surface [2]. This enhances the fatigue performance of specimens during service. Advantages of water jet shot peening include high energy density [3], cold processing [4], and being environmentally friendly [5]. The jet pressure, incidence angle, and position can be accurately controlled [6, 7]. The technology enables surface modification in areas that are hard to access through the adjustment of jet parameters [8]. Pulsating water jet (PWJ) forced decaying of the continuous water jet into discrete clusters to use the hammer effect. By periodically applying impact pressure in the form of a water droplet in a continuous stream to erode the material. Poloprudsky explored the erosion phenomenon during the PWJ impact, and observed the erosion damage evolution focusing on early erosion stages [9, 10]. Srivastava *et al* explored the modification of SS304 grade stainless steel by pulsating water jet process, and the surface residual stress increased from the initial 69 MPa to −540 MPa, and the microhardness also increased. They investigated the effects of PWJ on surface morphology, residual stress, etc, and explored its potential as a surface treatment process [11]. However, for high hardness materials, the impact pressure brought by pure water is limited. Water jet peening forms a mixed jet by adding a certain proportion of shot particles to the water, greatly improving its impact force on the surface of the sample. Compared to pure water impact, the modification effect on high hardness materials is more obvious. Compared to traditional pneumatic peening, water jet peening is more effective for treating high hardness specimens [12, 13] and has a higher energy utilization rate [14]. It holds great promise as a surface modification technique. According to the different mixing methods of water and shots, it is divided into suspension waterjet and injection waterjet [15]. Under the same pressure conditions, suspension waterjet can make shots obtain greater speed than injection waterjet. Like pneumatic peening, shots, coverage and intensity are three important factors of a mixed jet peening technology. The coverage of a mixed jet is affected by various

factors such as jet pressure, mixing ratio, and target material conditions. In addition, it is also a key factor affecting the surface integrity of a modified material [16].

To predict and control coverage, Kirk and Abyaneh [17–20] firstly proposed a theoretical model. The model links the indentation growth rate to coverage through the assumption of a constant impact rate of random shots on an infinitely large target surface. Based on this, Holdgate [21] developed another model that extends the existing model to describe the growth pattern of coverage involving multiple peening sources. Shahid *et al* [22] adopted an artificial neural network-based method to improve the accuracy of coverage recognition results. The experiments showed that this method was superior to previous standard image segmentation methods. Miao *et al* [23] proposed using the equivalent plastic strain value corresponding to U3 (the vertical displacement of the indentation position) as the critical value for determining whether coverage is achieved. Xiao *et al* [24] developed a theoretical equation for calculating random peening coverage. The results can be accurately calculated from impact density and average indentation size through probability theory. Nguyen *et al* [25] developed a three-dimensional unsteady peening simulation platform for coverage prediction based on the commercial computational fluid dynamics software ANSYS-FLUENT. This multi-phase peening enhancement simulation platform can be used to predict air peening flow and coverage.

In simulating the effect of coverage, Wu *et al* [26] discovered that as the coverage increased from 100% to 400%, surface CRS increased linearly. The maximum value of CRS barely increased after reaching 300% coverage. Yang *et al* [27] utilized finite element methods to simulate the CRS on Almen specimens and showed that as the coverage increased, the absolute values of both the maximum and surface CRS had a peak value. Lin *et al* [28, 29] found that increasing the coverage of shot peening can improve the maximum CRS value and the size of plastic strain, but has little effect on the thickness of the CRS layer and no obvious regularity on the roughness value. Pham *et al* [30] used finite element methods to find that coverage has a significant effect on the distribution of CRS in the AISI 4340 steel. Increasing coverage, shot speed, and shot size are effective methods for obtaining higher and deeper levels of CRS field. Qiang *et al* [31] applied a random finite element model to study the effect of coverage on Q345qD steel. The results showed that both the surface and maximum CRS exhibit nonlinear growth with increasing coverage. The surface roughness also has a corresponding rise.

In the coverage effect experiments and fatigue investigations, Pour-Ali and Liu [32, 33] realized that high coverage can cause grain refinement and form a certain thickness of the nano-crystalline layer on the stainless steel's surface. Maleki *et al* [34] investigated the impact of different coverage levels on the fatigue behavior of AISI 1050 low-carburized steel, and found that high coverage significantly improves the fatigue life of specimens. At the same time, it is also an effective way to obtain a nanostructured layer and superior mechanical performance [35]. Qin *et al* [36] explored the effects of 4 different shot peening coverage on the surface integrity and fatigue crack growth performance of 7B type aluminum sheets. The results showed that with the increase of coverage, both the surface hardness and CRS increased, and the fatigue crack growth rate firstly decreased and then increased. Li *et al* [37] examined the effect of coverage on the fatigue performance of the 7B75-T7751 alloy. The results indicated that the fatigue lifespan improves with higher coverage. However, excessively high coverage leads to formation of micro-cracks on surface and causes a decline in lifespan. Vielma *et al* [38] through fatigue tests on specimens with different coverages demonstrated that the overall lifespan was more than three times longer compared to untreated specimens. However, the effect of shot peening with low coverage (80%) was almost negligible. Sakamoto *et al* [39] discovered that fatigue limit of specimens with coverage ranging from 140%–2300% increased by 14%–25% compared to unprocessed specimens. The results indicate that valuable coverage of round bar is higher than full coverage, which can significantly improve the fatigue limit of the medium carburized steel.

Based on existing studies, there is lack of an accurate control experimental method of coverage, and there is also limited research on the constraints of high coverage. In this paper, we propose an analytical calculation method for coverage, and select a high-strength carburized steel (18CrNiMo7-6) as the study material to investigate the impact of different high coverages on its surface integrity. Then, an ideal coverage range is established to enhance the fatigue performance of material specimens.

2. Analytical calculation model of coverage

Figure 1(a) illustrates a schematic diagram of the suspension water jet process. In this process, shots are accelerated and impact the surface of the specimen, causing plastic deformation and reinforcing the surface of the specimens. Figure 1(b) shows a schematic diagram of the contact size of the indentations. The surface morphology after peening is shown in figure 1(c). As peening time increases, the number of indentations and coverage increase, but this growth is exponential. As coverage increases, the growth rate decreases. The relationship between coverage, impact rate, and time established by Kirk and Abyaneh [17–20] is expressed as

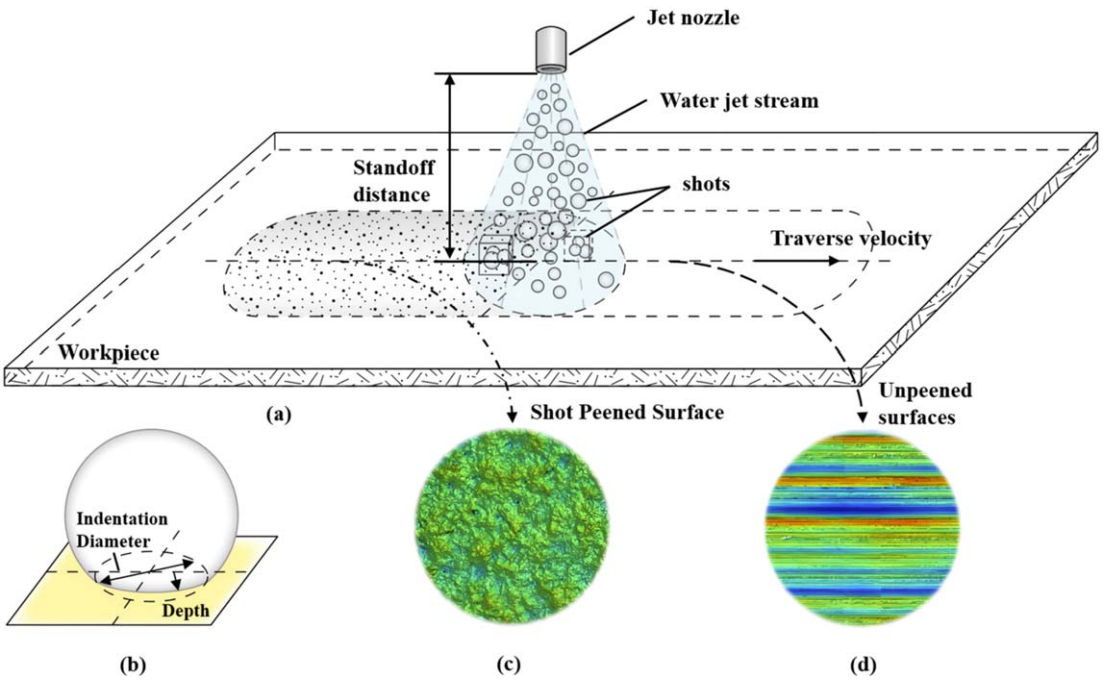

Figure 1. (a) Suspension waterjet strengthening, (b) contact size of impact indentation, (c) morphology of strengthened area, and (d) morphology of unpeened area.

$$C_{th} = 100\% \times [1 - \exp(-\pi r^2 R t)] \tag{1}$$

where r represents the average radius of the indentations on the surface after impact, R is the rate of generation of the indentation in a unit area, and t represents the peening time.

The formula mainly focuses on the trend of coverage and has the advantage of easy application with few input parameters. In order to obtain accurate coverage values under different process parameters, this paper proposes an analytical calculation method for coverage. The method is based on analyzing and exploring each factor that affects coverage change, including the theory of random distribution of shots, stream divergence angle, standoff distance, traverse speed, shot speed and mass flow rate etc. By using MATLAB to couple calculate these factors, simulate the jet peening process and predict the coverage and target material state under different process parameters, it is more precise and efficient than judging surface coverage by visual observation and empirical formulas in engineering practice.

The determination of the distribution of shots within a stream is hampered by the restrictions imposed by nozzle size and the high-speed motion of the shots. Previous research has frequently treated this distribution as a uniformly random pattern, which is supported by both theoretical and empirical models. Salvati [40] and Axinte [41, 42] have posited that the spatial distribution of shots along the radial position x may exhibit a Gaussian distribution, which can be described as

$$P_a(\chi_a) = \frac{1}{\sqrt{2\pi}\,\sigma_a} e^{-\frac{(\chi_a - \mu_a)^2}{2\sigma a^2}} \tag{2}$$

where σ and α respectively represent the standard deviation and mean value, and $P_\alpha$denotes the probability of χ_α, which is the velocity ratio.

In order to investigate the specific laws and values of the distribution, the three-dimensional morphology of specimens following peening was examined. It was found that the impact deformation caused by the shot flow on specimens perpendicular to the nozzle's direction of motion was approximately normally distributed, whereas the distribution along the direction of motion of the nozzle was approximately uniform, as depicted in figure 2(a). During the experiment, the inlet pressure and mixing ratio were maintained in a stable state, thus implying that the phenomenon was primarily caused by the distribution pattern of the shots in the stream. The shots in the water jet stream exhibit radial diffusion, with a higher density in the central region and lower density at the edges [43]. Consequently, with more shots concentrated near the central position, a larger plastic deformation occurs in the center region compared to the edge, resulting in an 'inverse normal distribution' pattern.

In a circular nozzle, the center of shot distribution is coincident with the center of the nozzle. Under certain process parameters, the mass flow rate of the system is obtained, allowing for the determination of the number of

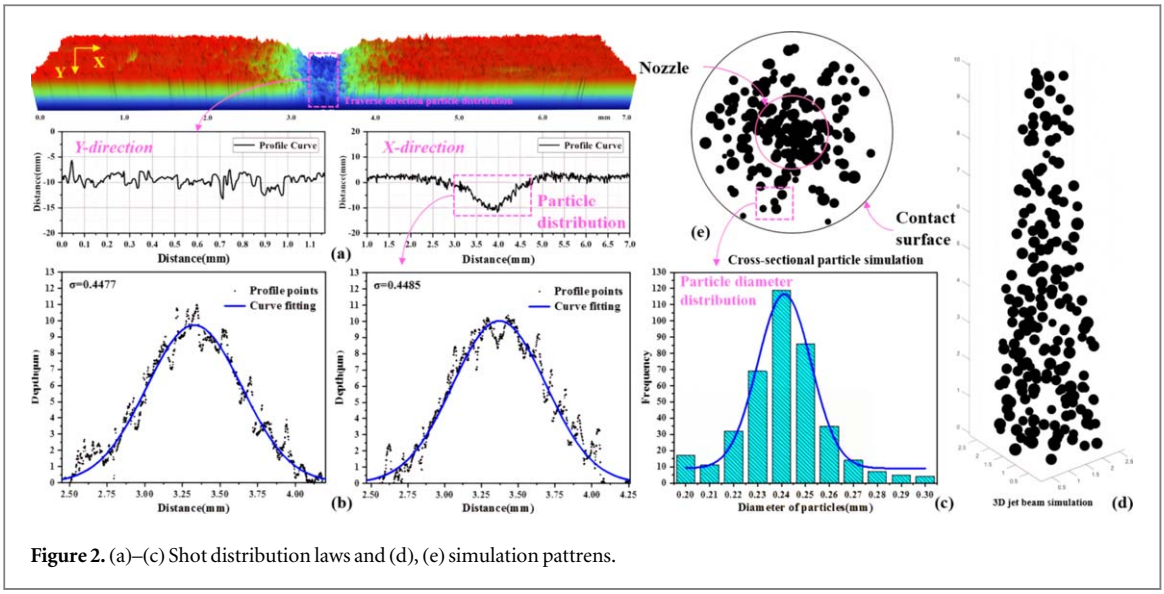

Figure 2. (a)–(c) Shot distribution laws and (d), (e) simulation pattrens.

Table 1. Distribution regularity experimental parameters.

No.	Inlet pressure P(MPa)	Traverse speed v_n(mm/s)	Standoff distance h(mm)	standard deviation σ
1	8	2	15	0.4364
2	8	0.2	15	0.4560
3	20	2	15	0.4404
4	20	0.4	15	0.4677
5	20	0.2	15	0.4159
6	20	0.1	15	0.4554
7	35	2	15	0.4842
8	35	0.2	15	0.4826

shots at each position by calculating the standard deviation of the normal distribution. The morphology of the specimens was then analyzed after exposure to different pressures. The experiment utilized a 1% water-shot mixture ratio. To facilitate easy detection and observation, a low nozzle velocity was employed. The displacement information of the morphologies under various parameters was extracted and processed using MATLAB software to calculate the standard deviation. The experimental parameters are presented in table 1.

As shown in figure 2(b), the fitting of the depression area morphology points displays a favorable trend. The standard deviation slightly increases with the growth of the inlet pressure, but the amplitude is not large. There is no obvious relationship between the standard deviation and the nozzle speed. The shots used in the experiment have been screened and the diameter size of the screened shots has been detected and statistically, the size distribution is shown in figure 2(d). The shot model parameters were defined based on this actual size distribution law.

The process of modeling using this method is depicted in figure 3. It assumes that each shot is generated randomly in any position within the space of the jet stream, and that each shot's impact on the target surface creates a circular depression. Total number of shots N in the region is calculated based on the process parameters, and the first shot model is created with its spatial coordinates determined using the MATLAB random function. Subsequent shots are generated in space according to the distribution law and undergo collision detection simultaneously to ensure that the shot distribution aligns with the actual peening process. The target area is thoroughly discretized and divided into a finite number of discrete point coordinates. The distance between each discrete point and the indentation center is calculated and compared to the indentation diameter, and coverage is obtained by counting the number of discrete points in various states.

The simulation results are shown in figure 2(c). The indentation size varies due to the different shot diameters and jet velocities. The calculation program cannot accurately determine the contact size of the indentations produced by different shot velocities. This aspect must be established through systematic experimentation and then incorporated into the calculation program.

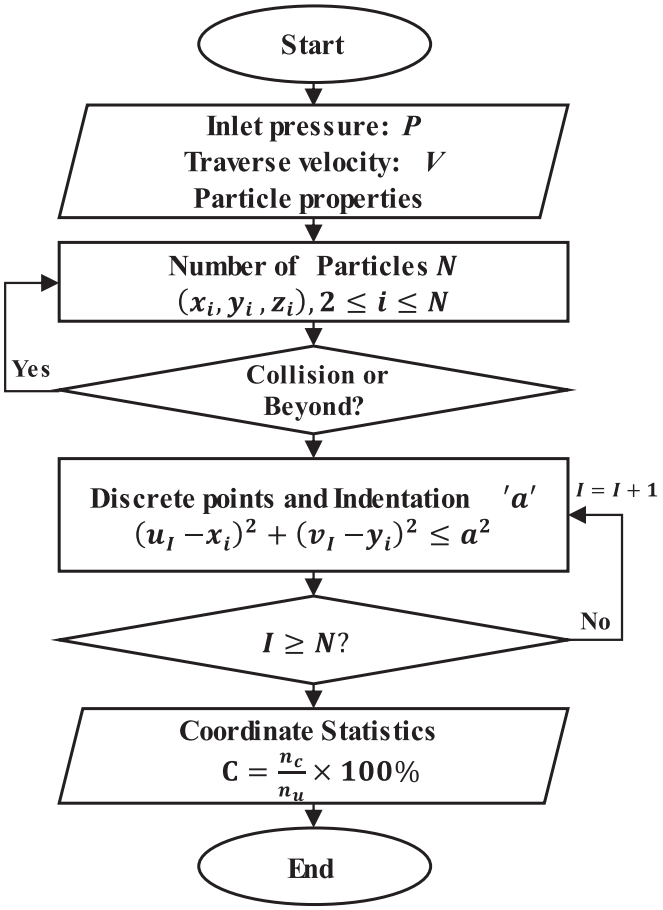

Figure 3. Parametric modeling flow chart.

Table 2. Chemical composition of 18CrNiMo7-6 steel (wt%).

Element	C	Si	Mn	S	P	Cr	Ni	Mo	Cu
Content	0.15–0.21	0.4	0.5–0.9	<0.035	<0.035	1.5–1.8	1.4–1.7	0.25–0.35	⩽0.3

3. Indentation size and coverage verification

3.1. Experimental materials and equipment

The experiment used 18CrNiMo7-6 carburized steel as the research object.18CrNiMo7-6 is a high-quality carburized steel that possesses high hardness and excellent mechanical properties on the surface after undergoing carburizing treatment. It finds widespread use in various industrial parts, particularly in the area of high-speed heavy-load gears [44–46]. The carburized steel was formed into block-shaped specimens with dimensions of 50 × 50 × 50 mm^3. The surface hardness was around 55–58 HRC after carburizing and the carburizing layer was 1.2 mm deep. Its chemical composition is presented in table 2 (mass fraction).

It is found that increasing the hardness, velocity and size of the shot is an effective method to obtain a higher level of residual stress and a deeper residual stress zone in the target material [30]. Therefore, the shot used is a high-strength steel wire cut shot produced according to DIN8201 standard, with a hardness of 750–850 HV, which is the hardest shot for the existing 0.2 mm diameter specifications. To reduce surface roughness and approach the theoretical model, the manufacturer carried out special polishing treatment on the steel wire cut shots used in experiments, dulling most of the sharp specimens. The chemical composition of the shot is listed in table 3.

A self-designed Suspension Waterjet Modification Device was utilized to modify the specimens (illustrated in figure 4). The device comprises a high-pressure water generation system, a suspension waterjet hydraulic system, and a motion control system. The suspension waterjet hydraulic system, depicted in figure 5, consists of a pure water branch and a shot branch, with pressure gauges (p_1, p_2, p_3, and p_4). The flow rate can be regulated by

Figure 4. Photograph of the suspension waterjet modification system.

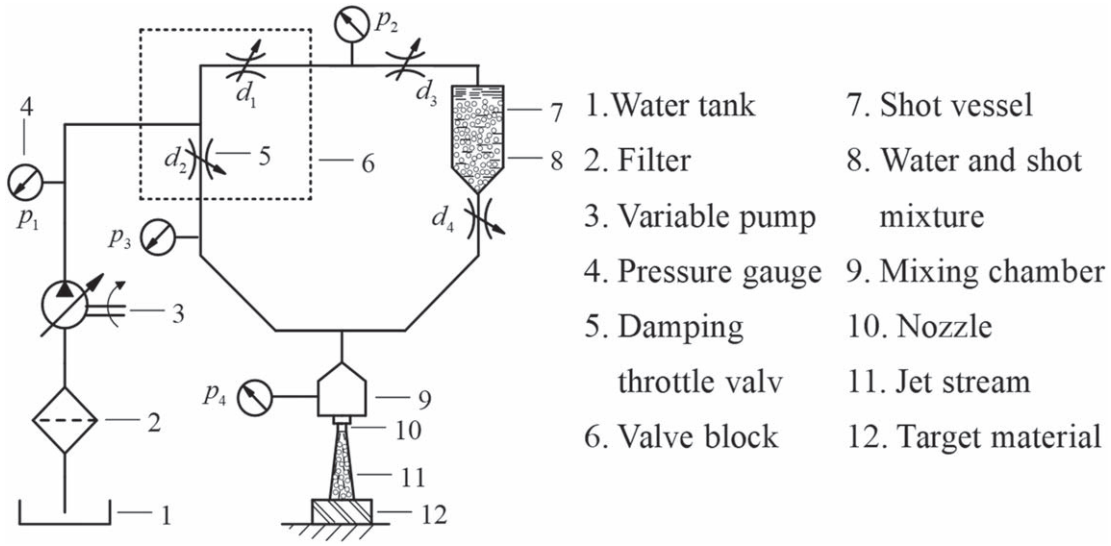

Figure 5. The working principle of the suspension waterjet system.

Table 3. Chemical composition of steel wire cutting shots (wt%).

Element	C	Mn	Si	S	P	Fe
Content	0.45–0.75	0.40–1.20	0.10–0.30	0.04	0.04	Bal

adjusting the speed of the variable pump. The modification pressure is achieved when the inlet pressure gauge (p_4) reaches the set indicator and the speed regulation is stopped. To further decrease the mixing ratio of the system, a series of damping holes (d_1 and d_3) have been installed at the inlet of the shot branch, and the sizes of the damping holes (d_1, d_2, d_3, and d_4) on each branch can be adjusted to effectively modify the jet's mixing ratio. The nozzle used in the experiment has an aperture of 1.2 mm and a length of 30 mm. The five-axis motion platform comprises of three linear axes (XYZ) and two rotational axes (AB). The XYZ axes control the spatial movement of the nozzle assembly with a repeat positioning accuracy of 0.02 mm, the B axis adjusts the nozzle assembly's angle with a swing range of $\pm 60°$, and the A axis, the main shaft, enables both speed and position control.

The microstructure of the specimens was analyzed using a QC-02 industrial microscope at 90 × magnification. The crystal residual stresses were determined using a high-power x-ray CRS analyzer, specifically the Proto-LXRD type. The Cr target K-alpha radiation and Fe (211) diffraction plane were used with the gaussian algorithm

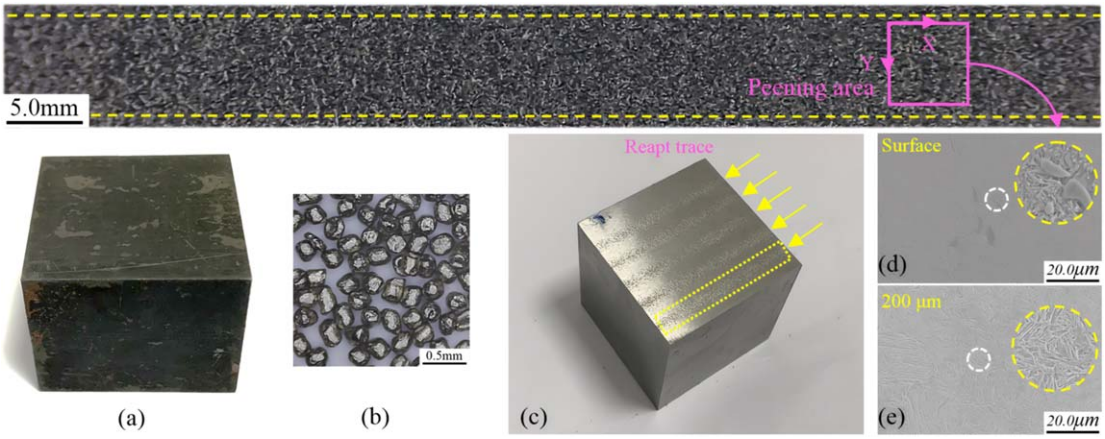

Figure 6. (a) Original specimen, (b) microscope of shot, (c) modified specimen surface, and (d, e) scanning electron microscope images of different positions after peening.

applied to fit the entire CRS field. Electrochemical corrosion was utilized for the peeling process, with a depth of 10 μm. The peeling depth was measured and corrected with the use of a micrometer. The three-dimensional morphology and surface roughness of the modified specimens were evaluated through non-contact measurement with an NPFLEX three-dimensional surface measurement system.

3.2. Indentation contact size experimental

In order to easily observe the indentation size on the material surface under certain standoff distance and inlet pressure conditions, the coverage of the specimen surface is minimized by increasing the nozzle speed and decreasing the mixing ratio. The mixing ratio is maintained at less than 0.05% during the experiment by adjusting the size of damping holes, and the range of the screened steel shots used is 0.200 to 0.315 mm. The speed of the water and shots in the jet can be controlled by adjusting the inlet pressure, and formula (3) describes the relationship between nozzle inlet pressure and speed [47]. Our research group, using Particle Image Velocimetry, found that the ratio of shot speed to fluid speed at the nozzle outlet is approximately 0.8, and the shot speed can be calculated using formula (4). The specimen surface is polished, and then straight-line peened under different pressures to establish the relationship between speed and indentation size.

$$v_{\mathrm{w}} = 44.72\sqrt{P} \tag{3}$$

$$v_s = 0.8v_{\mathrm{w}} \tag{4}$$

Where v_w is the speed of water, v_s is the speed of shots, and I is the nozzle inlet pressure.

The specimens used in the original experiment are displayed in figure 6(a), while the shots utilized are presented in figure 6(b). In order to guarantee the accuracy of the experiment results, five tracks were processed on specimens within the same experimental group and indentation morphology was analyzed at different positions (figure 6(c)). After undergoing peening with a specified coverage, the specimen surface was imaged using a scanning electron microscope, as shown in figure 6(d). The plastic deformation layer caused by the shot impact is clearly visible on the surface. The high carburized content results in numerous small white carburized particles and residual austenite in the picture. The core of the specimen, as seen in figure 6(e), reveals a higher presence of martensite, with a scarcity of residual austenite and carburized particles that are barely noticeable.

After experiments, the surface morphology of a specimen was analyzed using an industrial microscope (figure 7(a)), which revealed that the surface was filled with a number of indentations of varying sizes. By utilizing a three-dimensional surface measuring system, the morphology and contact size of indentations were assessed (figure 7(b)). Figures 7(c) and (d) present the data of indentation morphology and size under a pressure of 20 MPa. The indentation morphology under pressures of 1 to 35 MPa is depicted in figure 8. As the pressure increased, the shot speed and kinetic energy increased, leading to more prominent traces on the specimen surface. At a pressure of 1 MPa, indentations were not sufficient to conceal the surface grinding marks, but when the pressure increased to 4 MPa, the edges of indentations appear 'accumulation' due to material extrusion. As the pressure continues to rise, the mass flow of the system Q increases, leading to a higher impact rate R, which in turn results in an increase in the number of visible indentations on the specimen surface.

The indentation size was recorded and analyzed under various velocities (as shown in figure 8(b)). Fifty indentation data points were collected for each experimental condition, and the size distribution was fitted to a normal distribution using MATLAB software. By comparing the size distribution of the experiment shots (as

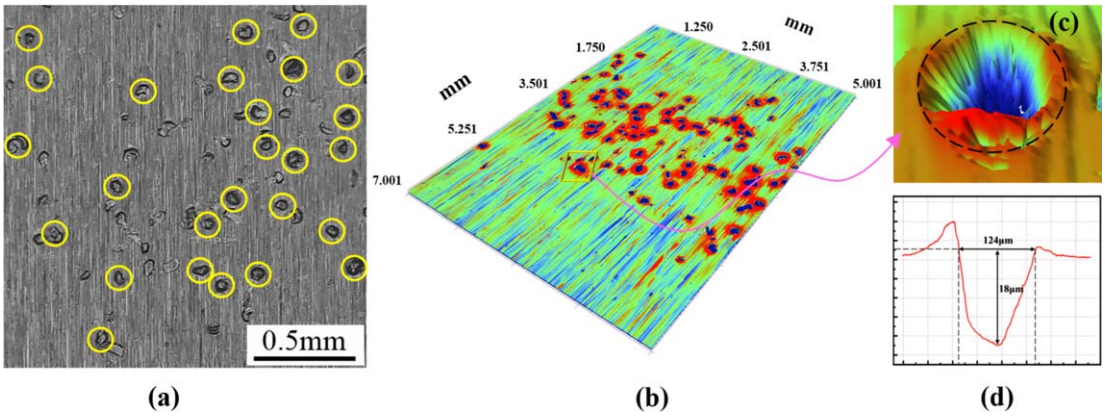

Figure 7. (a) Microphotograph of indentation under 20 MPa pressure, (b) 3D morphology map, (c) single indentation morphology, and (d) single indentation size.

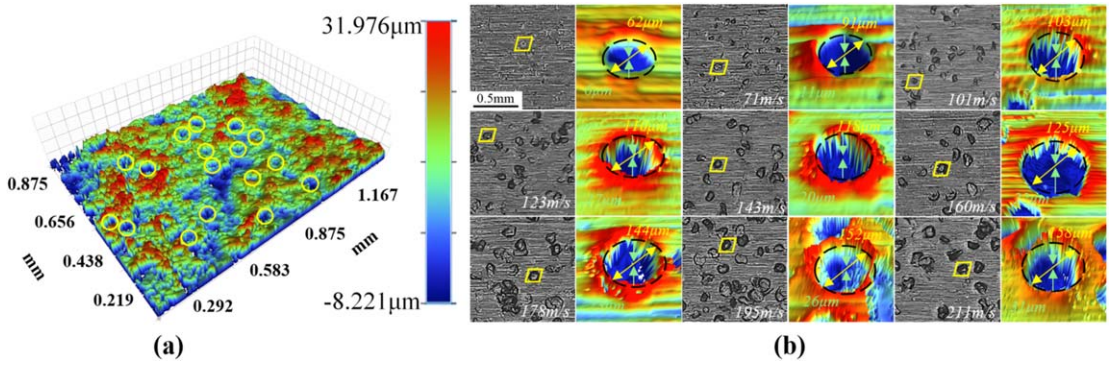

Figure 8. (a) Indentation detection location and (b) indentation morphology under different pressures.

Table 4. Coverage verification experimental parameters.

No.	Experimental inlet pressure P(MPa)	Traverse speed v_n(mm/s)	Calculated coverage C_t(%)	Experimental coverage C_ε(%)
1	19.9	80	12.9004	14.76
2	20.5	70	15.2280	16.93
3	20.3	60	18.5173	20.14
4	20.5	50	20.4176	23.36
5	20.6	40	23.4790	24.91
6	20.3	30	30.5680	29.68
7	20.6	20	47.4554	42.35
8	20.6	10	64.6437	61.12
9	20.2	5	90.4035	91.69
10	20.4	1	96.5782	96.78

shown in figure 2(d)), the values for the indentation size caused by shots of different pressures and diameters could be determined (as shown in figure 9).

3.3. Coverage verification experiment

With the support of the above experimental results, the coverage is calculated by the program under certain process parameters. At the same time, the specimen is experimented according to the process parameters to verify the accuracy of the coverage calculation program. Due to the difficulty of detecting coverage above 98%, the experiment mainly focuses on verifying coverage below 98%. After validation, the coverage under different process parameters is obtained through the program. The experiment parameters are listed in table 4.

A 1×2 mm^2 central region was chosen as the coverage detection area. To ensure the stability of the results, the coverage was detected at 4 different locations for each group of identical parameters, and the average value was selected as the final coverage. The left column of figure 10 is a perspective view of the simulated parameter

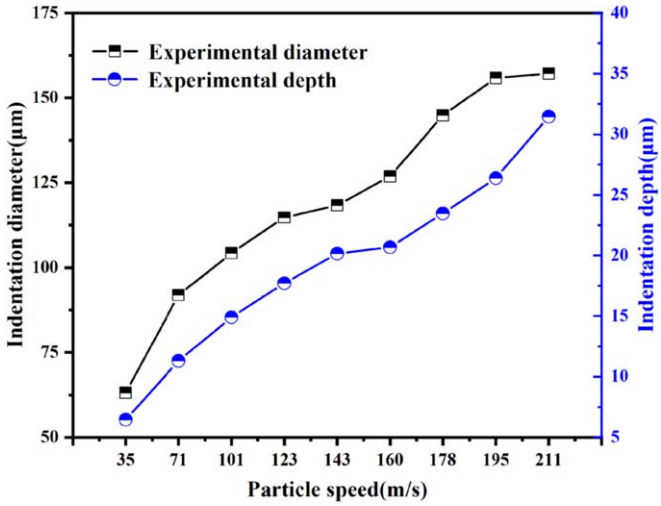

Figure 9. Indentation size under different velocities.

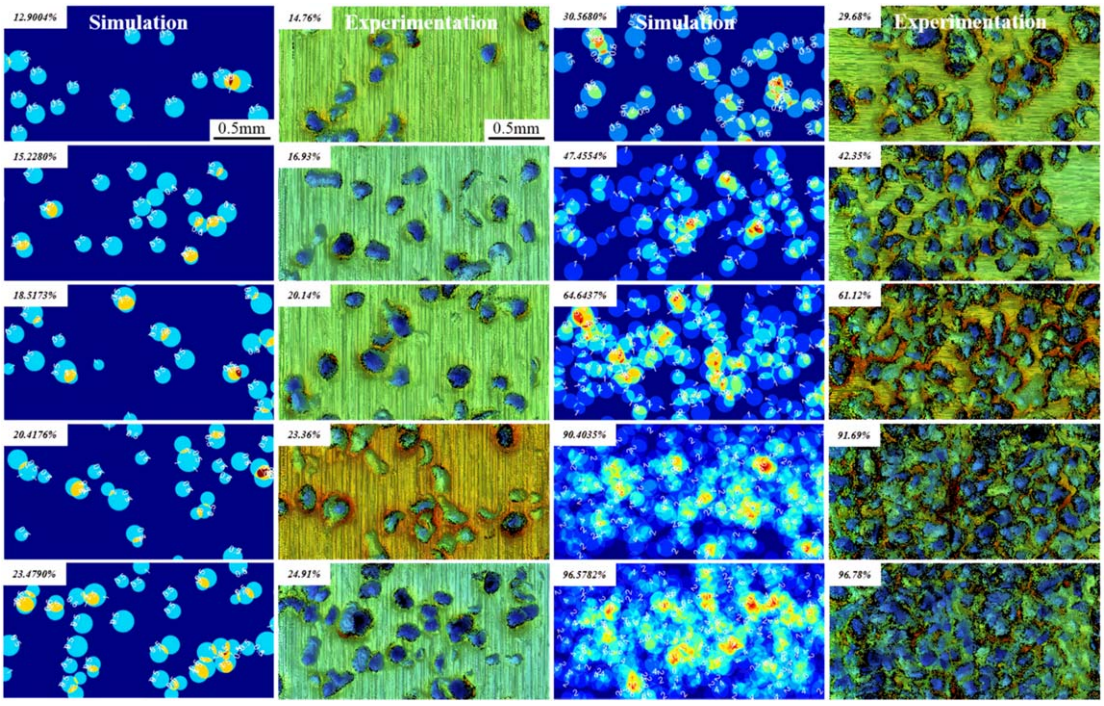

Figure 10. Theoretical and experimental coverage comparison chart.

for coverage, with the color ranging from 'blue' to 'red' indicating the increasing number of times that the area was impacted by shots, and the white lines indicating the number of impacts for the same state areas. As the nozzle speed is decreased, the coverage area expands, and when overage is low, there are fewer overlapping indentations. As coverage increases, the number of overlapping indentations increases, and the concentration of repeated impacts in the center is significantly higher than in the edge area.

Python was used to classify the experimental results images to determine the coverage values. The experimental morphology is depicted in the right column of figure 10.

The comparison between the simulated and experimental coverage at different speeds is shown in figure 11(a). The simulated coverage aligns well with the experimental results, with an error margin of less than 6%, and the maximum error in the analytical coverage is 10%. The highest experimental error is 17%, which supports the validity of the analytical coverage method and the indentation parameters. The analytical and experimental coverages at four different locations under each set of identical parameters were tested. The average value was selected as the final coverage.

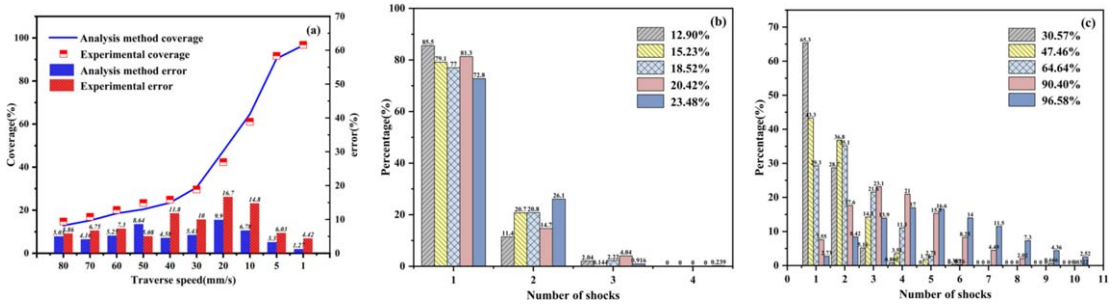

Figure 11. (a) Analytical and experimental coverage comparison and (b), (c) the proportion of strikes at different coverages.

Table 5. Experimental parameters.

Parameter name	Parameter symbols	Parameter value	Parameter units
Nozzle diameter	D	1.2	mm
Shot diameter	D_1	0.2	mm
Stream angle	θ	90	°
Standoff distance	T	15	mm
Mixture ratio	M	9–10	%
Shot flow rate	Q	1.91–2.06	Kg·min^{-1}

Figures 11(b) and (c) respectively depict the distribution of impact times in the simulated group under varying coverage levels. When coverage is low, impact times are primarily concentrated at a single instance, with shots mainly impacting un-impacted areas. As coverage increases, shots increasingly impact areas near the center, resulting in a wider range of impact times and a shift towards higher frequency times, ultimately resulting in an impact time distribution that approximates a normal distribution. At 90.40% coverage, the impact time distribution closely resembles a normal distribution with a mean of 3, while at 96.58% coverage, it closely resembles a normal distribution with a mean of 4, due to the expansion of the distribution range, its 'standard deviation' is significantly higher than the former.

4. The impact of coverage on the surface integrity of carburized steel

4.1. Surface morphology and roughness

In engineering, 98% coverage is often considered complete, and peening time that is double the original (or half the traverse speed) is equivalent to 200% coverage. Using the above coverage analytical model as support, a single factor experiment was conducted to examine the effect of various coverages on the surface integrity of carburized steel. The experiment adjusted the traverse speed to alter the coverage. Previous research carried out by our group indicated that both excessively high and low jet intensities are detrimental to modification, and the optimal results can be achieved when the inlet pressure within the range of 16–25 MPa (shots velocity of 143–178 m s^{-1}) [48]. As a result, the pressure was fixed at 20 MPa for this experiment. The standoff distance was set at 15 mm to maximize jet stream energy utilization. The specimens were peened in a straight line under specified process parameters. The experiment parameters are listed in table 5.

As depicted in figure 12, with the rise of coverage, the material surface becomes increasingly rough and plastic deformation progressively increases. When coverage is 8,000% or below, the distribution of indentations is relatively uniform, with small and dense indentation traces easily visible on the specimen surface. However, as coverage reaches 10,000%, there are obvious local depressions near the central position of the specimen, which are larger than the indentation traces caused by a single shot and gradually expand with the increase of the coverage. To gain an accurate understanding of the coverage and progression of local damage.

To accurately understand the coverage rate of local damage, figure 13 shows the ultra-depth electron microscopy and electron microscopy images of surface when the coverage rate exceeds 10,000%. It is observed that damage on the surface morphology of the specimen due to excessively high coverage rate can be roughly divided into four stages. When the coverage rate increases from 10,000% to 16,000%, local depressions appear

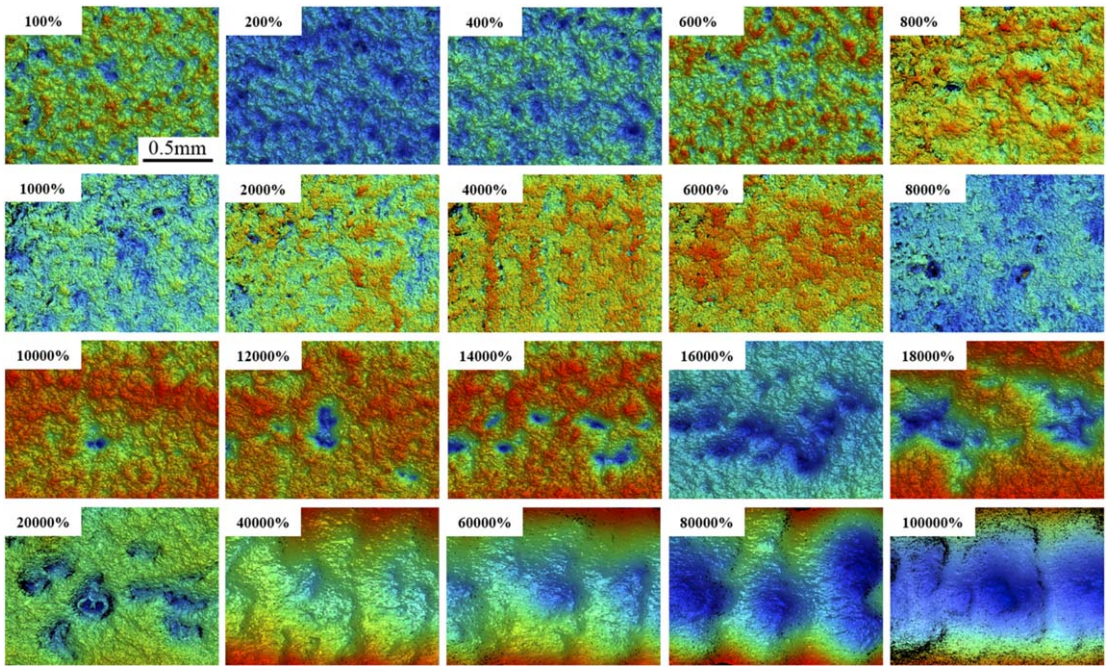

Figure 12. The effect of different coverages on surface morphologies.

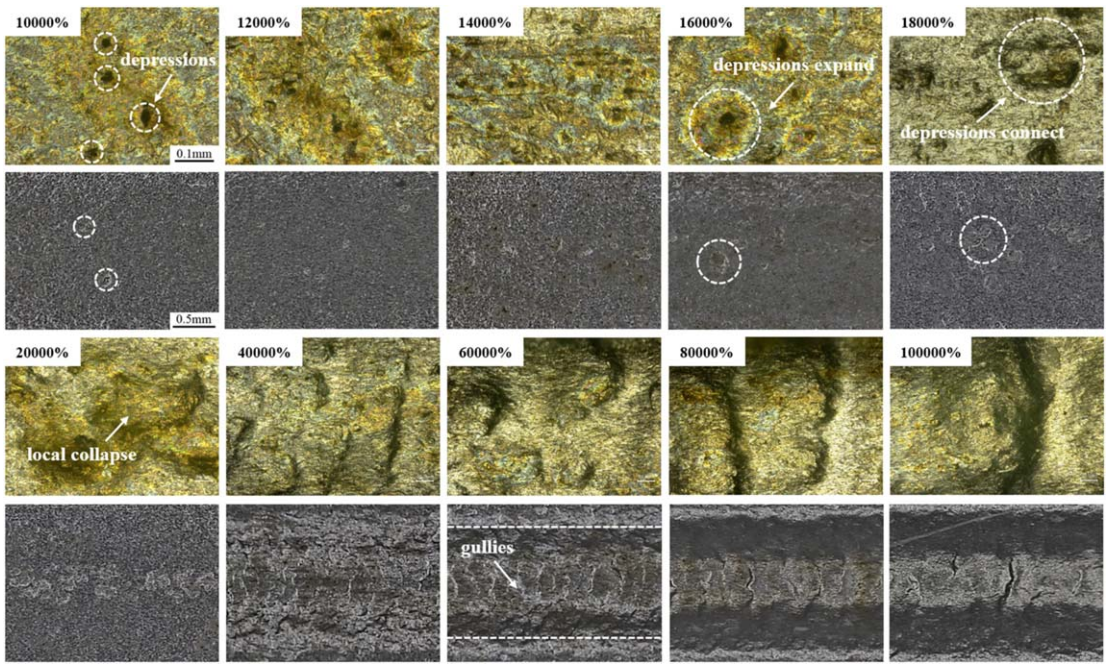

Figure 13. The ultra-depth electron microscopy images under different stages of damage.

on surface and gradually expand as the coverage rate increases. When the coverage rate reaches around 18,000%, depressions gradually connect with each other. When the coverage rate approaches 20,000%, the connected depressions form a local collapse. Finally, when the coverage rate exceeds 20,000%, the surface is severely damaged, and the central area is eroded and worn, forming 'egullies'.

This is because when the coverage is high, the number of repeated impacts of shots increases. The impacts not only cause overlap effects but also remove surface material. At the same time, internal material generated by pressure will create noticeable protrusions at the impact edges and form local depressions. Since shots spread radially within the water jet stream, the density of impacts is higher in the central area and lower at the edge. As the number of impacts near the depressions increases significantly, the depressions will merge with material

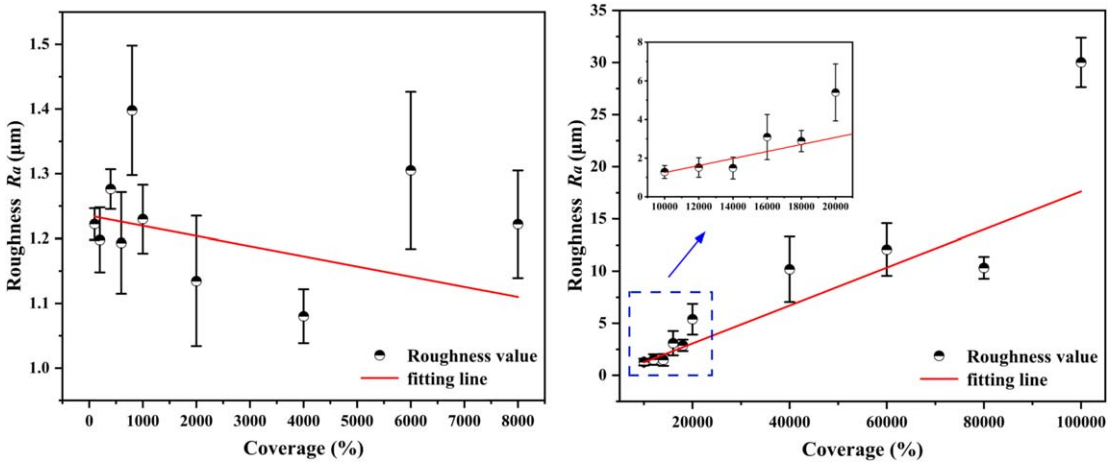

Figure 14. The change in roughness under different coverages.

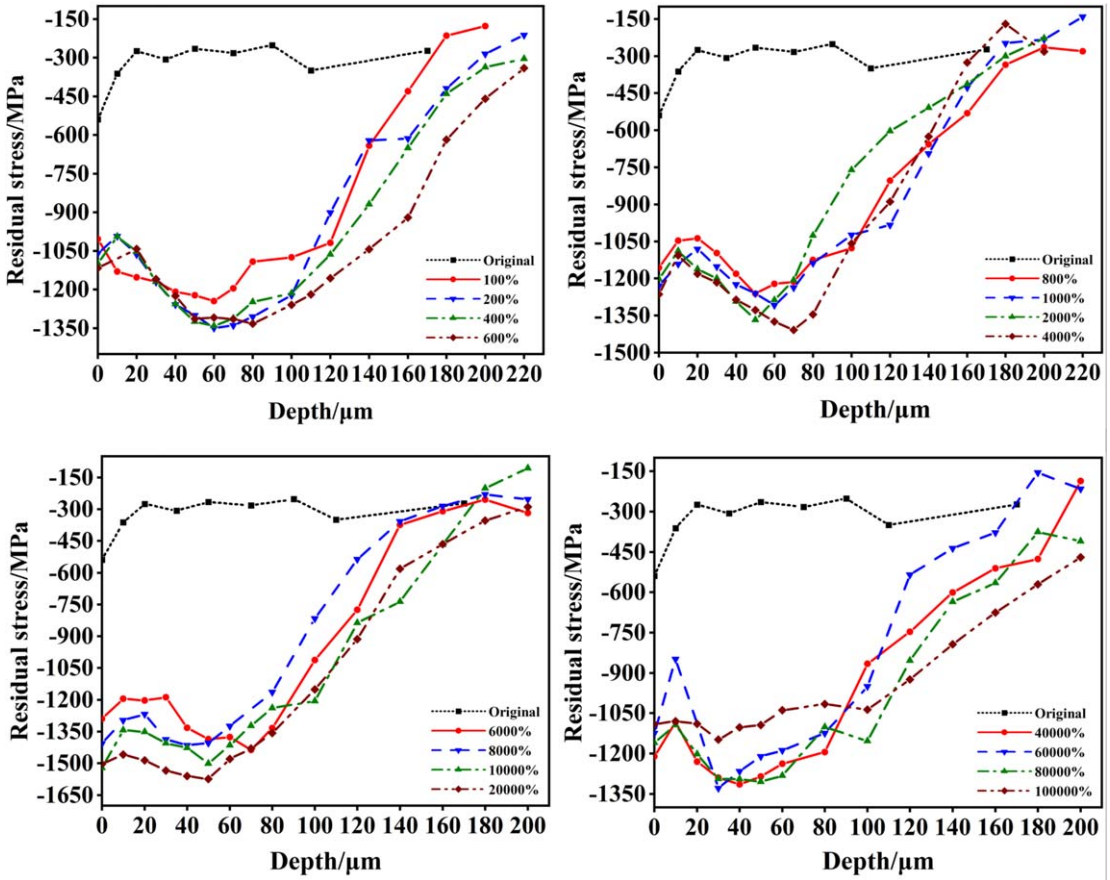

Figure 15. Compressive residual stress field under different coverages.

compression marks, causing the plastic deformation area to gradually expend until forming 'gullies'. This will have a negative effect on the surface morphology and roughness of the material.

The surface roughness of the specimen changes under varying coverage, as depicted in figure 14. The NPFLEX three-dimensional surface measurement system was used to accurately measure the surface roughness of the modified specimen. In order to ensure the accuracy of roughness parameters under each group of experimental conditions, six different positions were sampled under the same pass, and the average value of these six parameters was taken as the roughness value. The difference between the average and maximum values of each parameter was used as the boundary band of coverage error. The roughness can be categorized into two

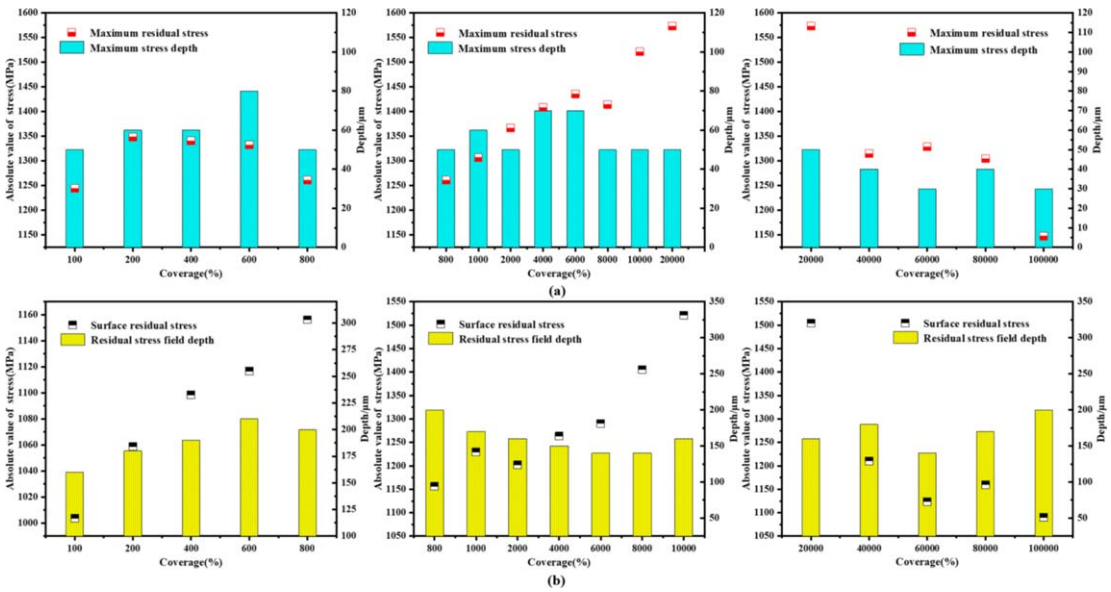

Figure 16. (a) The change in the maximum residual compressive stress and its depth and (b) the change in the surface residual compressive stress and the field total depth under different coverages.

phases. During the initial stage, when coverage increases from 100% to 8,000%, the roughness value (Ra) fluctuates around 1.2 μm. The fitted line shows a slight downward trend, but it is not significant. In the latter stage, as coverage continues to rise from 10,000% to 100,000%, roughness demonstrates a rising trend with increasing coverage. This rise becomes significantly steeper when coverage surpasses 20,000%. This is evident from the impact of coverage on the specimen's surface morphology. To maintain a defect-free surface and ensure appropriate roughness, the coverage of the carburized steel should be kept within 8,000% when the modification pressure is constant.

4.2. Compressive residual stress field

The modified specimens exhibit high compressive residual stress both on the surface and at a certain depth, as demonstrated by the CRS curves in figure 15. The distribution of the entire CRS field displays a 'spoon-shaped' pattern, with the surface and maximum CRS reaching above −1000 MPa. As coverage increases, there are noticeable alterations in the surface and maximum CRS of specimens.

The relationship between the coverage and maximum CRS and surface CRS is illustrated in figure 16. The maximum CRS can be roughly categorized into three phases (figure 16(a)): unstable, enhancement, and decrease. As the coverage increases from 100% to 800%, the trend in the maximum CRS change is not obvious, exhibiting fluctuations around −1300 MPa. Despite this, the depth of the maximum CRS layer remains relatively constant at around 60 μm. As the coverage increases from 800% to 20,000%, the maximum CRS shows a gradual increase. At a coverage of 800%, the maximum CRS is −1261 MPa, which rises to −1573 MPa at 20,000% coverage, representing an increase of 24.7%. Despite this upward trend, the depth of the maximum CRS layer remains around 60 μm. It is speculated that the increase in coverage leads to the accumulation of plastic deformation, causing the maximum CRS at the material to rise. However, the constant inlet pressure and the difficulties in energy transfer from the specimen surface to deeper positions result in limited effect of coverage on the depth of the CRS field. As the coverage increases from 20,000% to 100,000%, the specimen's maximum CRS experiences a rapid decrease, dropping from −1573 MPa to −1147 MPa, a decrease of 27.6%. Additionally, the depth of the maximum CRS decreases to 30 μm. This can be attributed to 'over peening', a phenomenon caused by excessive erosion and wear on the surface due to the high number of shots impacting the material.

The effect of coverage on surface CRS is sensitive, as shown in figure 16(b). It can be divided into two phases, the ascending phase and the declining phase. When coverage rises from 100% to 10,000%, surface CRS experiences a significant upward trend, rising from −1003 to −1521 MPa, a 51.6% increase. As coverage continues to rise from 10,000% to 100,000%, surface CRS drops to −1038 MPa, a 31.8% decrease. This is because as coverage increases, plastic deformation at the surface leads to accumulated work hardening, resulting in a substantial rise in material surface CRS. However, when coverage becomes too high, erosion and wear from

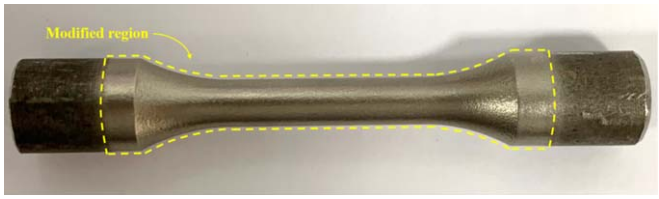

Figure 17. A modified round bar specimen.

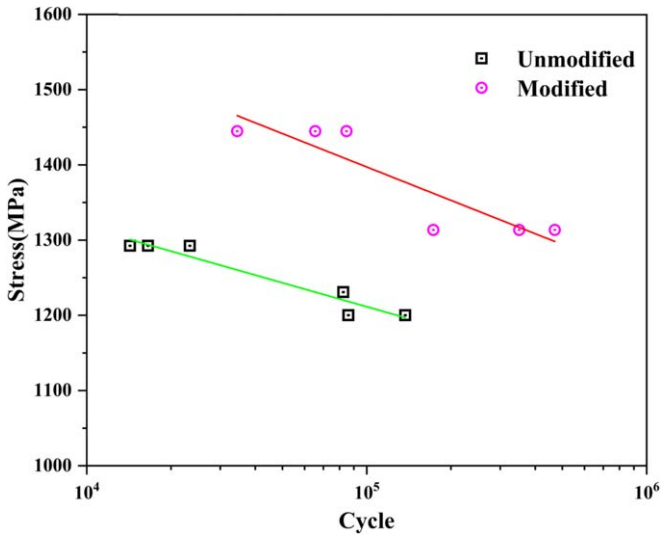

Figure 18. Comparison of fatigue behavior between modified and unmodified round bar specimens.

'over peening' cause surface destruction, causing a rapid decrease in surface CRS. The effect of coverage on total CRS layer depth is not substantial and generally remains around 175 μm.

5. Discussion

This study investigates the precise control method for coverage and its effect on the surface integrity of carburized steel. An analytical calculation method for coverage was proposed and verified, and can be applied to other materials. Coverage, as one of the two key elements in peening, significantly affects surface integrity parameters and may vary for different materials. For 18CrNiMo7-6 carburized steel, the optimal coverage range is between 1,000%–8,000%, with 1,000% coverage being the best choice as it balances peening efficiency and surface integrity. Under this condition, although the surface and the maximum CRS value have not reached the maximum, they have all reached a stable state, which can meet the modification requirements of the specimen and the roughness is minimal.

Fatigue damage occurs in three stages: crack formation, crack propagation and final fracture. From this point of view, the fatigue life of a material is directly related to its surface properties such as hardness, metallurgical features, notch effects etc, because a fatigue crack usually starts on surface. In this respect, if the suitable surface treatment is applied, the fatigue life of a material can be improved [49, 50]. Shot peening is a process that induces work-hardening on surface and forms a residual stress field in the component's surface layer, thereby suppressing occurrence of surface stress concentration and transferring the surface crack source to sub-surface. This effectively enhances the service life of the component. The Institute of Fatigue Resistance at Zhengzhou University conducted research to assess the influence of waterjet modification with 1,000% coverage on fatigue round bar specimen. The modified round bar specimens are shown in figure 17. The Nakamura test (figure 18) revealed that the modified specimens displayed a 150 MPa higher failure stress compared to the unmodified specimens after 10^4–10^6 fatigue cycles. This test demonstrates the significance of selecting an appropriate coverage for enhancing the fatigue performance of specimens.

The advantage of water jet peening lies in its ability to precisely control jet pressure, incidence angle, and injection location, making it easy to apply in engineering. By adjusting the jet parameters, surface modification of small, narrow parts that withstand alternating loads, such as gear roots, threads and blade roots, which are difficult to process with traditional machining, can be achieved. However, these small areas require fine nozzles and fine shot to achieve modification. Therefore, more stringent parameters and schemes need to be developed for surface modification of these areas.

6. Conclusions

An analytical method was employed to determine the coverage of suspension waterjet peening, and a single factor experiment was conducted to investigate the effect of coverage on the surface integrity of 18CrNiMo7-6 carburized steel. The conclusions can be summarized as follows

(1) The validity of the analytical method for calculating coverage was established and found to be effective in predicting the coverage and impact state of the material surface under varying process parameters. The impact indentation size and shot distribution pattern were identified as key factors affecting coverage.

(2) As coverage increased from below 10,000%, fluctuations in surface roughness (Ra) were observed, though remained within a range of 1.2 μm. Beyond 10,000% coverage, roughness exhibited a continuous upward trend, with a sharp increase noted when coverage exceeded 20,000%.

(3) Both surface CRS and maximum CRS showed an upward trend with increasing coverage, reaching peak enhancements of 51.6% and 24.7%, respectively. However, when coverage exceeded a certain level, the 'over peening' phenomenon caused both values to decrease and the depth of maximum CRS to diminish. The impact of coverage on the total depth of CRS was minimal.

(4) The fatigue tests on standard specimens modified with 1,000% coverage demonstrated that an appropriate coverage level can effectively avoid surface damage and defects, resulting in a significant enhancement of the specimen's service life.

Acknowledgments

This work was supported by the National Natural Science Foundation of China (No. U1804254) and the Natural Science Foundation of Henan Province (No. 21A460024).

Data availability statement

All data that support the findings of this study are included within the article (and any supplementary files).

ORCID iDs

Ning Sun https://orcid.org/0000-0003-2627-8003
Chunsheng Lu https://orcid.org/0000-0002-7368-8104

References

[1] Arola D, McCain M L, Kunaporn S and Ramulu M 2001 Waterjet and abrasive waterjet surface treatment of titanium: a comparison of surface texture and residual stress *Wear* **249** 943–50
[2] Ramulu M, Kunaporn S, Jenkins M, Hashish M and Hopkins J 2001 Fatigue performance of high-pressure waterjet-peened aluminum alloy *J. Pressure Vessel Technol.* **124** 118–23
[3] Azhari A, Schindler C, Kerscher E and Grad P 2012 Improving surface hardness of austenitic stainless steel using waterjet peening process *Int. J. Adv. Manuf. Technol.* **63** 1035–46
[4] Haghbin N, Spelt J K and Papini M 2015 Abrasive waterjet micro-machining of channels in metals: comparison between machining in air and submerged in water *Int. J. Mach. Tools Manuf* **88** 108–17
[5] Anwar S, Axinte D A and Becker A A 2013 Finite element modelling of overlapping abrasive waterjet milled footprints *Wear* **303** 426–36
[6] Arola D, Alade A E and Weber W 2006 Improving fatigue strength of metals using abrasive waterjet peening *Mach. SCI. Technol* **10** 197–218
[7] Kim T, Lee H, Kim M and Jung S 2012 A 3D FE model for evaluation of peening residual stress under angled multi-shot impacts *Surf. Coat. Technol.* **206** 3981–8
[8] Marini M, Piona F, Fontanari V, Bandini M and Benedetti M 2020 A new challenge in the DEM/FEM simulation of the shot peening process: the residual stress field at a sharp edge *Int. J. Mech. Sci.* **169** 105327

[9] Jakub P *et al* 2021 Surface and subsurface analysis of stainless steel and titanium alloys exposed to ultrasonic pulsating water jet *Materials* **14** 5212
[10] Poloprudský J, Chlupová A, Kruml T and Hloch S 2021 Identification of local microplasticity on Ti6Al4V after impingement of periodically acting water clusters *Advances in Manufacturing Engineering and Materials II* **ICMEM 2021** 63–74
[11] Srivastava M *et al* 2019 Surface integrity and residual stress analysis of pulsed water jet peened stainless steel surfaces *Measurement* **143** 81–92
[12] Saravanan S, Vijayan V, Suthahar S T J, Balan A V, Sankar S and Ravichandran M 2020 A review on recent progresses in machining methods based on abrasive water jet machining *Mater. Today Proc.* **21** 116–22
[13] Natarajan Y, Murugesan P K, Mohan M and Liyakath Ali Khan S A 2020 Abrasive water jet machining process: a state of art of review *J. Manuf Process* **49** 271–322
[14] Kavya J T, Keshavamurthy R and Kumar G S P 2016 Studies on parametric optimization for abrasive water jet machining of Al7075-TiB2in-situ composite *IOP Conf. Ser.: Mater. Sci. Eng.* **149** 012024
[15] Tazibt A, Parsy F and Abriak N 1996 Theoretical analysis of the particle acceleration process in abrasive water jet cutting *Comp. Mater. Sci.* **5** 243–54
[16] Bagherifard S, Ghelichi R and Guagliano M 2012 On the shot peening surface coverage and its assessment by means of finite element simulation: a critical review and some original developments *Appl. Surf. Sci.* **259** 186–94
[17] Kirk D and Abyaneh M Y 1993 Theoretical basis of shot peening coverage control *Proc. of the 5th Int. Conf. on Shot Peening* 183–90
[18] Kirk D and Abyaneh M Y 1995 Theoretical basis of shot peening coverage control *The Shot Peener* **9** 28–30
[19] Kirk D and Abyaneh M Y 1999 Theoretical basis of shot peening coverage control *The Shot Peener* **13** 5–7
[20] Kirk D 1995 Shot peening *Aircr. Eng. Aerosp. Technol.* **71** 349–61
[21] Holdgate N M D 1993 Peen mechanics in the shot peening process *PhD thesis* University of Cambridge
[22] Shahid L and Janabi-Sharifi F 2019 A neural network-based method for coverage measurement of shot-peened panels *Neural Computing and Applications* **31** 4829–36
[23] Miao H Y, Larose S, Perron C and Lévesque M 2009 On the potential applications of a 3D random finite element model for the simulation of shot peening *Adv. Eng. Softw.* **40** 1023–38
[24] Xiao X, Tong X, Gao G, Zhao R, Liu Y and Li Y 2018 Estimation of peening effects of random and regular peening patterns *J. Mater. Process. Tech.* **254** 13–24
[25] Nguyen V B, Poh H J and Zhang Y 2014 Predicting shot peening coverage using multiphase computational fluid dynamics simulations *Powder Technol.* **256** 100–12
[26] Wu J, Liu H, Wei P, Lin Q and Zhou S 2020 Effect of shot peening coverage on residual stress and surface roughness of 18CrNiMo7-6 steel *Int. J. Mech. Sci.* **183** 105785
[27] Yang Z, Lee Y, He S, Jia W and Zhao J 2020 Analysis of the influence of high peening coverage on almen intensity and residual compressive stress *Appl. Sci.* **10** 105
[28] Lin Q, Liu H, Zhu C, Chen D and Zhou S 2020 Effects of different shot peening parameters on residual stress, surface roughness and cell size *Surf. Coat. Technol.* **398** 126054
[29] Lin Q, Liu H, Zhu C and Parker R G 2019 Investigation on the effect of shot peening coverage on the surface integrity *Appl. Surf. Sci.* **489** 66–72
[30] Pham T Q, Khun N W and Butler D L 2017 New approach to estimate coverage parameter in 3D FEM shot peening simulation *Surf. Eng.* **33** 687–95
[31] Qiang B, Li Y, Yao C and Wang X 2018 Effect of shot peening coverage on residual stress field and surface roughness *Surf. Eng.* **34** 938–45
[32] Pour-Ali S, Kiani-Rashid A, Babakhani A and Virtanen S 2018 Severe shot peening of AISI 321 with 1,000% and 1,300% coverages: a comparative study on the surface nanocrystallization, phase transformation, sub-surface microcracks, and microhardness *International Journal of Materials Research* **109** 451–9
[33] Liu H, Wei Y, Tan C K I, Ardi D T, Tan D C C and Lee C J J 2020 XRD and EBSD studies of severe shot peening induced martensite transformation and grain refinements in austenitic stainless steel *Mater. Charact.* **168** 110574
[34] Maleki E, Unal O and Kashyzadeh K R 2018 Effects of conventional, severe, over, and re-shot peening processes on the fatigue behavior of mild carbon steel *Surf. Coat. Technol.* **344** 62–74
[35] Maleki E and Unal O 2018 Roles of surface coverage increase and re-peening on properties of AISI 1045 carbon steel in conventional and severe shot peening processes *Surf. Interfaces* **11** 82–90
[36] Qin, Li B, Zhang H, Youani Andre Wilfried T, Gao T and Xue H 2022 Effects of shot peening with different coverage on surface integrity and fatigue crack growth properties of 7B50-T7751 aluminum alloy *Eng. Fail. Anal.* **133** 106010
[37] Li B, Xue H, Sun Z, Qin Z and Zhang H 2021 Influence of surface coverage on the fatigue behavior of a shot peened AA7B50-T7751 alloy *Surface Topography: Metrology and Properties* **9** 35041
[38] Vielma A T, Llaneza V and Belzunce F J 2014 Effect of coverage and double peening treatments on the fatigue life of a quenched and tempered structural steel *Surf. Coat. Technol.* **249** 75–83
[39] Sakamoto J, Lee Y and Cheong S 2014 Effect of shot peening coverage on fatigue limit in round bar of annealed medium carbon steel *J. Mech. Sci. Technol.* **28** 3555–60
[40] Salvati E, Lunt A J G, Heason C P, Baxter G J and KorSunsky A M 2020 An analysis of fatigue failure mechanisms in an additively manufactured and shot peened IN 718 nickel superalloy *Mater. Design* **191** 108605
[41] Axinte D A, Karpuschewski B, Kong M C, Beaucamp A T, Anwar S, Miller D and Petzel M 2014 High energy fluid jet machining (HEFJet-Mach): from scientific and technological advances to niche industrial applications *CIRP Ann.* **63** 751–71
[42] Mieszala M, Torrubia P L, Axinte D A, Schwiedrzik J J, Guo Y, Mischler S, Michler J and Philippe L 2017 Erosion mechanisms during abrasive waterjet machining: model microstructures and single particle experiments *J. Mater. Process. Tech.* **247** 92–102
[43] Balz R 2011 Determination of spatial velocity distributions of abrasive particles in abrasive water jets using laser-induced fluorescence under real conditions *2011 WJTA-IMCA Conference and Expo (Houston, Texas, September 19-21, 2011)*
[44] Wu J, Liu H, Wei P, Lin Q and Zhou S 2020 Effect of shot peening coverage on residual stress and surface roughness of 18CrNiMo7-6 steel *Int. J. Mech. Sci.* **183** 105785
[45] Qin S, Zhang C, Zhang B, Ma H and Zhao M 2022 Effect of carburizing process on high cycle fatigue behavior of 18CrNiMo7-6 steel *Journal of Materials Research and Technology* **16** 1136–49
[46] Pöhl F 2020 Local deformation and transformation behavior of retained austenite in 18CrNiMo7-6 after high-carbon carburizing treatment *Mater. Charact.* **167** 110446
[47] Momber A W 2001 Energy transfer during the mixing of air and solid particles into a high-speed waterjet: an impact-force study *Exp. Therm Fluid Sci.* **25** 31–41

[48] Ma Y T *et al* 2022 Effect of pre-mixed jet velocity on surface roughness and residual stress of 18CrNiMo7-6 carburized steel *Aeronautical Manufacturing Technology* **65** 14–20
[49] Yetim A F *et al* 2023 Tribological behavior of plasma-sprayed Yttria-stabilized zirconia thermal barrier coatings on 316L stainless steel under high-temperature conditions *Materials Letters* **336** 1338973
[50] Yetim A F *et al* 2023 A comprehensive study on the fatigue properties of duplex surface treated Ti6Al4V by plasma nitriding and DLC coating *Surf. Coat. Technol.* **458** 129367